ELSEVIER

Journal of Power Sources 79 (1999) 169–183

JOURNAL OF POWER SOURCES

One-dimensional thermal model for direct methanol fuel cell stacks Part I. Model development

P. Argyropoulos, K. Scott *, W.M. Taama

Chemical and Process Engineering Department, University of Newcastle upon Tyne, Merz Court, Newcastle upon Tyne NE1 7RU, UK

Received 24 August 1998; accepted 27 December 1998

Abstract

A thermal energy model for the direct methanol fuel cell (DMFC) is presented, based on the differential thermal energy conservation equation. The model is used to predict the thermal behaviour of a DMFC stack comprising of many large cells in a bipolar arrangement. The model allows an assessment of the effect of operating parameters (feed and oxidant inlet temperature, flow rate and pressure, operating current density), and the system design (active area, material properties and geometry) on the temperature profile along the stack and the interactions between the various components in the cell stack. The model is designed to enable the fuel cell system designer to estimate, insulation requirements, auxiliary equipment sizing and required thermal duties and response. Furthermore, the model can be used to decide on the optimum set of operating conditions for an efficient thermal management of the whole process.

Keywords: Fuel cell; Direct methanol; Thermal modelling; Thermal energy balance

1. Introduction

A fuel cell stack consists of a number of single cells usually connected electrically in series. Typically the stack is composed of several components.

(1) Two stainless steel end plates, which are used to align and compress the stack, two Teflon sheets which isolate the end plates from aluminium or copper current collector plates.

(2) Membrane electrode assemblies (MEA) consisting of two catalysts, one as cathode the other as anode, attached to the polymer electrolyte membrane (PEM), which serves both as cell separator and electrolyte. Two carbon-backing layers serve as support for the uncatalysed gas diffusion layers and for the catalyst layer in each.

(3) Bipolar plates, for fuel and oxidant flow, which have flow channels machined on both surfaces and are in electrical contact with the carbon backing layer.

The MEA are sandwiched between the bipolar plates. The membrane is electrically insulated at its sides to avoid a cell short-circuit. This insulation material (Teflon tape) also serves as a seal for the cell. The repeated section: bipolar plate–flow channels–carbon backing layer–uncatalysed layer–anode catalyst layer–membrane–cathode catalyst layer–uncatalysed layer–carbon backing layer constitutes the fuel cell stack. The last two graphite plates in the stack are different to the bipolar plates, as they have channels machined on only one side, the other side is in direct contact with the current collector.

Several attempts have been made to develop thermal models for PEM fuel cells (e.g., Refs. [1–9]). These models are for hydrogen, oxygen fuel cells and typically treat the cell stack as a process unit, trying to develop models based on electrical performance and the inlet–outlet streams physical characteristics, without focusing on the different stack components. There is no information provided about heat transfer through the various cell compartments and the interactions between them. Thus, it is not possible to determine the operating temperatures of the various components in the fuel cell and thus to fully

* Corresponding author

0378-7753/99/$ - see front matter
PII: S0378-7753(99)00181-0

assess the influence of temperature on the cell performance. Thus, this paper presents a thermal energy model for the direct methanol fuel cell (DMFC), based on the differential thermal energy conservation equation. The model will be used to predict the thermal behaviour of a DMFC stack comprising of many large cells in a bipolar array and to predict the variation in temperature of the components within the cell.

A large scale DMFC stack (25 cells of 272 cm^2 active area each) is currently being built at Newcastle. As part of that development effort we have developed a series of engineering models concerning DMFC stack thermal management, individual cell and overall system pressure drop, and reactants/products flow distribution [10–14]. These steady state models were based on a number of simplifying assumptions, and their main aims were to help the understanding of the processes that occur inside a DMFC system, their interactions, and their effect on the overall system behaviour. This then enables assessment and/or improvements to be made on system design, optimal operating conditions, and to the sizing of auxiliary equipment (pumps, coolers, heaters, tanks) requirements to operate a DMFC fuel cell stack.

The thermal model presented is part of an overall modelling and scale up study of the DMFC. The ultimate goal is to merge all the four aforementioned models into a global engineering model that will be used to describe the prototype DMFC stack system under development in Newcastle. The present model will be enriched with the addition of a hydrodynamic model that describes the flow distribution through the manifolds and inside the cells, a chemical equilibrium model predicting local conditions and physical properties based on reactants/products mixture composition. It is expected that the accuracy of such a model will be satisfactory and comparable with the experimental data that will be collected from our prototype stack. In the long term such a model will be used to describe the dynamic response of such a stack.

2. Reversible, irreversible and total heat losses for DMFCs

A fuel cell is an electrochemical system in which the chemical energy of the fuel (in this case methanol) is converted directly into electrical energy with the aid of an oxidant (usually air). Under the assumption that the cell is working isothermally, then, during the cell reaction and, depending on the magnitude and direction of the entropy change, enthalpy flows will occur. This change will be negative if the enthalpy flow is to the surroundings. According to the second law of thermodynamics, for reversible processes we have:

$$\Delta Q_{rev} = T\Delta S = \Delta H - \Delta G \quad (1)$$

where ΔQ_{rev} is the reversible change in thermal energy in J, T is the absolute temperature, ΔS is the entropy change, ΔH is the enthalpy change, and ΔG is the Gibbs free energy change.

In practice, the cell reaction is irreversible and so both the anode and the cathode reactions experience overpotentials which in some cases can be considerable. Moreover, the conductivity of the solid polymer electrolyte (Nafion® 117 in our case) is finite and is the cause of heat production when electrical current is generated.

The irreversible losses in fuel cells lead to waste heat generation ($\dot{Q}$), which may be expressed by:

$$\dot{Q} = -\frac{T\Delta Si}{nF} + i\Sigma\eta + i^2R. \quad (2)$$

In this equation, the first term represents the entropic loss, which cannot be overcome due to thermodynamic considerations, the second term is due to activation and mass transfer overpotentials, and the third is due to ohmic heating effects [15]. The pressure must also be specified for a complete definition of the thermodynamic states of the products and reactants. If the same pressure is chosen for both reactions then the heat of reaction is equal to the enthalpy change [16]. This is the case for the DMFC.

3. Cell characteristics

The reactions that occur in the DMFC are: the anode side,

$$CH_3OH + H_2O \rightarrow 6e^- + 6H^+ + CO_2$$

and at the cathode,

$$\frac{3}{2}O_2 + 6e^- + 6H^+ \rightarrow 3H_2O$$

which can be combined and give the overall reaction:

$$CH_3OH + \frac{3}{2}O_2 \rightarrow 2H_2O + CO_2.$$

To represent cell characteristics suitable anode and cathode polarisation data is required. Such data will, in general, depend on the structure and catalyst used in the cell. The thermal model developed here is designed to accommodate general cathode and anode overpotential behaviour and thus it is suitable to use published galvanostatic polarisation data [17]. This data refers to a liquid feed DMFC operating at 70°C and 4 bar oxygen overpressure [18,19]. This data, shown in Fig. 1, is one of the most accurate available in the open literature and hence is suitable to use in modelling the liquid fed DMFC. The data are for five methanol solution concentrations (0.5–2.5 M, step of 0.5 M) and hence the model can only be used accurately only for this five cases. The data were converted to continuous functions (for use in the computer model), which are plotted in Fig. 1 against the measured values, with the aid of a curve fitting program (Curve Expert v. 1.34). The fitting was with a sixth degree Lagrangian polynomials, which are particularly well suited for data sets with a low number of data

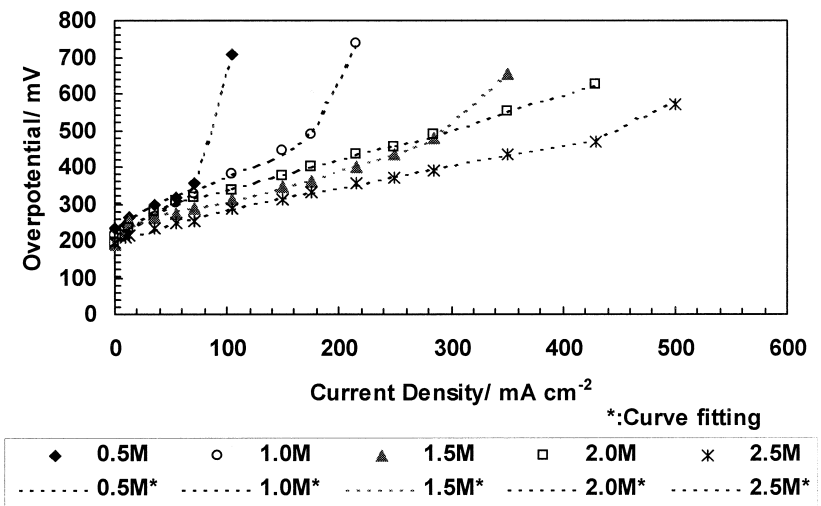

a) Anode overpotential

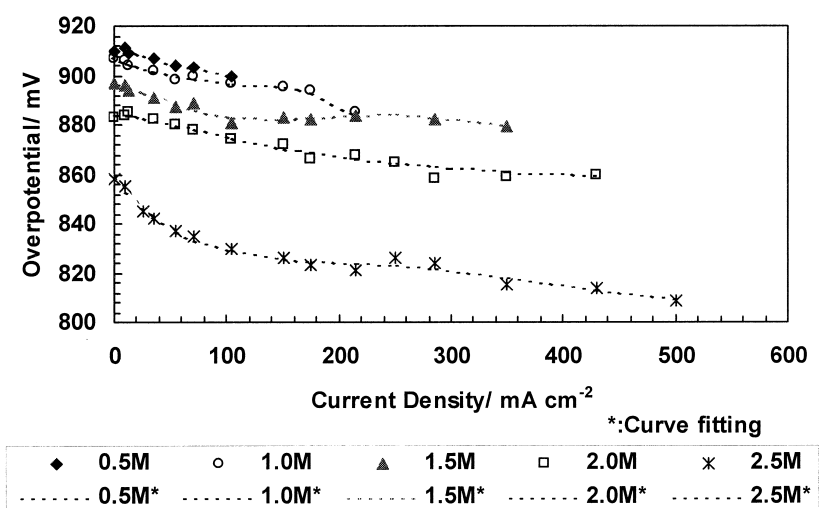

b)Cathode overpotential

Fig. 1. Anode and cathode side galvanostatic polarisation data as reported from Ravikumar [18] and Ravikumar and Shukla [19] (70°C cell temperature, 4 bar oxygen pressure).

points (eight or less). Like all polynomials, the Lagrangian interpolating polynomial exhibits more oscillatory behaviour as the degree increases. Therefore, the use of Lagrangian interpolations should be avoided if the number of data points is large.

The following equations describe the enthalpy of reaction and the enthalpy balance for both anode and cathode half cell reaction, in which we consider that the enthalpy change for the formation of electrons is zero [20]. We use the concept of single electrode reaction enthalpy changes due to the fact that the electrode are separated by the SPE membrane which acts as both a source of thermal resistance and of internal enthalpy generation due to its electrical resistance. This approach will allow us to determine more accurately the temperatures in the anode and cathode layers and in the membrane.

$$\Delta H_a = \left[N_{MeOH}(\Sigma H_{f,a}^{\circ} - \Sigma G_{f,a}^{\circ}) \right] + \left[(\bar{T}_{acl} - 298.15)\left(m_{MeOH}\bar{c}_{p,MeOH} + m_{CO_2}\bar{c}_{p,CO_2} - m_{H_2O}\bar{c}_{p,H_2O} \right) \right] \quad (3)$$

$$\Delta H_c = \left[N_{O_2}(\Sigma H_{f,c}^{\circ} - \Sigma G_{f,c}^{\circ}) \right] + \left[(\bar{T}_{ccl} - 298.15)\left(-m_{O_2}\bar{c}_{p,O_2} + m_{H_2O}\bar{c}_{p,H_2O,vapor} \right) \right] \quad (4)$$

where m_I is the mass of stoichiometrically defined mass of reactants/products, H_f° and G_f° are the standard heats of formation and Gibbs free energies (products–reactants) of the electrode reactions. Enthalpies of formation and Gibbs free energies of reactions are tabulated in Appendix A [16,21].

Thermodynamicists commonly use the 'Electron Convention' which treats the electron as a standard chemical element with an enthalpy of formation defined as zero at all temperatures. For electrons in ionised gases a value of 6.2 kJ mol^{-1} at 298 K (or 5/2 RT) is also in use. For the enthalpy of proton formation a value of -1170 kJ $equivalent^{-1}$ [22] is recommended but there is still dispute about this subject. The effect of the enthalpy of proton (or solvated proton) formation is to influence the maximum temperature in the membrane because protons are formed in the anode catalyst layer and consumed at the cathode catalyst layer. The enthalpy of vaporisation for water and methanol is calculated by using the Prizer acentric factor correlation as presented by Reid et al. [23].

4. Thermal modelling development

The thermal model is developed on the basis that the total inlet flow rate is equally divided in all the cells present in the stack. The flow bed design used for the present model is a simple one with each cell having 57 rectangular channels of equal depth and width.

To describe the distribution of temperature in a DMFC stack the following assumptions are made to simplify the mathematical treatment.

- Catalysts layers are thin compared to the membrane, and act as either heat source or heat sink and no concentration gradient exists.
- The membrane has a high thermal resistance and joule heat is liberated into both fluids.
- Heat is transferred by electroosmotic flow of water and methanol across the membrane from anode to cathode.
- The surface of the graphite plate is in direct contact with the carbon cloth so we assume that both surfaces are at the same temperature.
- The channels are shallow and thus there is no temperature gradient between the top and the bottom.
- Anode and cathode streams are acting as heat transfer fluids and determine the amount of heat carried away from the cell.
- Liquid water and methanol are vaporised in the cathode side catalyst layer where there is sufficient heat for phase change to take place.

The model assumes that the anode and cathode streams are essentially well mixed and that they remove heat from the cell at their exit temperatures. The temperature distribution in the cell stack is one dimensional, parallel to the direction of current flow.

4.1. Anode gas diffusion layer

The anode gas diffusion layer is typically made from carbon cloth or paper. In our research the material is 'A' type carbon cloth manufactured by E-TEK. This is a plain weave cloth, weight of 116 g m^{-2} and thickness of 0.35 mm. The cloth has good mechanical strength and longer durability, than carbon paper, for use in the DMFC. On one side of the cloth a thin layer of carbon/Teflon paste is spread out evenly and forms the uncatalysed diffusion layer. Essentially the only net heat production in this layer is due to ohmic heating of the carbon-based material of the backing layer. The electrical conductivity of this material is relatively high and thus the potential drop through the structure will be small. So it should be expected that the associated heat generated by Joule heating will also be relatively small. A schematic representation of the thermal model for this part of the stack is presented in Fig. 2.

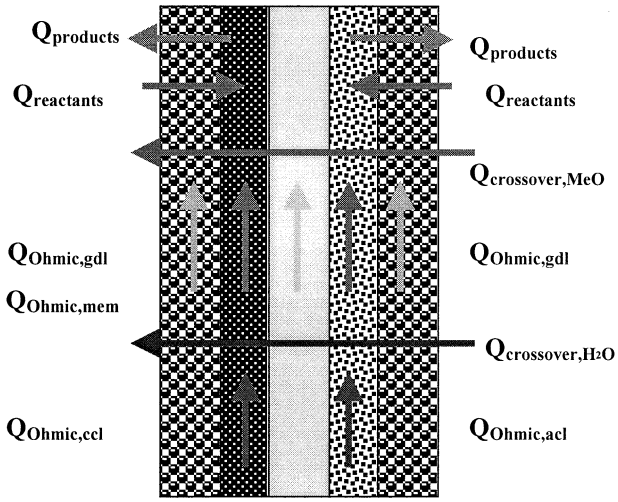

Fig. 2. Schematic representation of the MEA thermal model.

Overall, the carbon backing layers can be initially modelled as regions with a uniform effective conductivity in which linear conduction takes place and convective heat transfer, in which the dominant factor is that associated with the electroosmotic flow of water and methanol:

$$K_{\mathrm{agdl}}\frac{\mathrm{d}^2T}{\mathrm{d}x^2}+\sum_i \dot{m}_{i,\mathrm{agdl}}\bar{c}_{\mathrm{p},i}\frac{\mathrm{d}T}{\mathrm{d}x}=-i^2R_{\mathrm{agdl}} \tag{5}$$

where R_{agdl} is the ohmic resistance per unit volume, and i is the corresponding current. The above equation is valid under the assumption that heat losses to the surrounding environment, i.e., from the edge of the layer are negligible due to the small thickness of that layer (30 μm or less).

4.2. Anode catalyst layer

The anode catalyst layers are composites of Pt/Ru–C powder and ionomer. The enthalpy changes associated with the electrocatalytic reaction mean that temperature changes will occur in the catalyst layer. These temperature changes depend upon the rates of heat conduction and convective heat transfer associated with water and methanol electroosmotic transport.

The differential equation that describe the temperature profile in this section is:

$$K_{\mathrm{acl}}\frac{\mathrm{d}^2T}{\mathrm{d}x^2}+\left(\dot{m}_{\mathrm{H_2O,crossover}}\bar{c}_{\mathrm{p,H_2O}}+\dot{m}_{\mathrm{MeOH,crossover}}\bar{c}_{\mathrm{p,MeOH}}+\sum_i \dot{m}_i\bar{c}_{\mathrm{p,m},i}\right)\frac{\mathrm{d}T}{\mathrm{d}x}+\left(i\eta_{\mathrm{a}}+i^2R_{\mathrm{acl}}-\frac{i(\Delta H_{\mathrm{a}}-\Delta G_{\mathrm{a}})}{nF}\right)=0 \tag{6}$$

where η_{a} is the anode catalyst layer overpotential, ΔH_{a} is the anodic half cell reaction enthalpy (see Eq. (3)), ΔG_{a} is the Gibbs free energy, and R_{acl} is the ohmic resistance of the layer per unit volume.

4.3. Membrane

The solid PEM modelled is assumed to be Nafion® 117 from DuPont, as used in the majority of experimental programs. Modelling of the membrane, of thickness l_{m}, is based on the following assumptions.

- A fully hydrated continuum with effective ionic and electronic conductivities.
- Heat conduction defined by effective thermal conductivity $K_{\mathrm{eff,mem}}$.
- Heat transfer takes place mainly through the bulk (electroosmotic) flow of liquid (water and methanol).
- Heat losses to the surrounding environment are small due to the negligible thickness of the membrane.
- Joule heating occurs due to membrane ohmic resistance.

The energy balance for the membrane is:

$$K_{\mathrm{mem}}\frac{\mathrm{d}^2T}{\mathrm{d}x^2}+\left(m_{\mathrm{H_2O,drag}}c_{\mathrm{p,H_2O,m}}+m_{\mathrm{MeOH,drag}}c_{\mathrm{p,MeOH,m}}\right)\frac{\mathrm{d}T}{\mathrm{d}x}=-i^2R_{\mathrm{m}} \tag{7}$$

where R_{m} is the ohmic resistance per unit volume.

Typical characteristics of the Nafion® 117 membrane material are: thickness 175 μm, and effective thermal conductivity $k_{mem} = 0.21$ W m^{-1} K^{-1} [8].

The electroosmotic drag of water across the membrane, i.e., the number of water molecules that are dragged with each H^+ ion, depends on the membrane material and temperature [18,19,22–28]. Values vary between two and five although a most widely accepted value is approximately 2.5, which will be used in the model development. Thus, the mass of water that is dragged with protons is:

$$M_{H_2O,crossover} = \frac{2.5 j A_{mea} MW_{H_2O}}{10^3 n_e F}. \quad (8)$$

According to a model presented by Scott et al. [29] and Cruickshank and Scott [30] the methanol crossover rate can be approximated as:

$$m_{MeOH,crossover} = \frac{0.0164 j A_{mea} MW_{MeOH}}{10^3 n_e F}. \quad (9)$$

4.4. Cathode catalyst layer

Proton transfer across the polymer electrolyte to the cathode catalyst layer region will carry with it water and methanol. As, in the steady state, the water transferred from the anode plus that generated by reaction must equal that discharged into the cathode vapor phase (with also some liquid water production), there will be a relatively large variation in water 'concentration' in this layer. This is because at the vapor side of the catalyst layer ($x = 0$) there is zero current flowing from the electrolyte to the catalyst and thus zero ionic (proton) flow and consequently zero electroosmotic flow. Water is removed at this point by its effective diffusion rate. In principle, this situation requires a model for water transfer and the associated reactions. However, we assume that the local rate of water generation, predominantly in the vapor phase, is essentially constant and proportional to the overall current density j_T.

The differential equation that gives the temperature profile in this section is:

$$K_{ccl}\frac{d^2T}{dx^2} + \left(\dot{m}_{H_2O,crossover}\bar{c}_{p,H_2O} + \dot{m}_{MeOH,crossover}\bar{c}_{p,MeOH} + \sum_i \dot{m}_i \bar{c}_{p,m,i}\right)\frac{dT}{dx} + \left(i\eta_c + i^2 R_{ccl} + \frac{i(\Delta H_c - \Delta G_c)}{nF} - \Delta H_{vapor,H_2O} - \Delta H_{vapor,MeOH}\right) = 0 \quad (10)$$

where ΔH_c is the enthalpy of the cathodic reaction, ΔG_c is the Gibbs free energy, ΔH_{H_2O} is the enthalpy for liquid water vaporisation (electroosmotically dragged and reaction produced), ΔH_{MeOH} is the enthalpy of liquid methanol vaporisation, R_{ccl} is the ohmic resistance per unit volume. It should be pointed out that under the model assumptions all the liquid phase water and the liquid methanol that passes through the layer is vaporised as there is sufficient heat production in this layer to provide the required energy for the phase change. We ignore any oxidation of methanol at the cathode at this stage of the model development.

4.5. Cathode gas diffusion layer

The cathode gas diffusion layer model is similar to that already described above for the cell anode diffusion layer:

$$K_{cgdl}\frac{d^2T}{dx^2} + \sum_i \dot{m}_{i,cgdl}\bar{c}_{p,i}\frac{dT}{dx} = -i^2 R_{cgdl} \quad (11)$$

where R_{cgdl} is the ohmic resistance per unit volume.

4.6. Bipolar plates

Bipolar plates are currently made from non-porous carbon or resin impregnated graphite blocks. They are suitably impermeable to gas and liquid and have high electrical conductivity, corrosion resistance and mechanical strength. On either side of the block there are machined flow channels [31]. The bipolar plates provide the electrical connection between the cells and also act as the main heat transfer area between the cells. The MEAs are compressed between two bipolar plates, which means that each carbon cloth is in direct contact with the surface of the plate, and ideally with negligible contact

resistance. So as a first approximation we consider that the surface temperature of the bipolar plate and the carbon cloth is the same. The second important assumption of the present model is that the two fluids (methanol solution for the anode and air for the cathode) in steady state operation act as heat transfer medium, which add/remove heat from the main stack body. Heat is transferred from the three plate surfaces, which form the channel, and from the fourth surface of the carbon cloth. It is assumed that heat is transferred by the same mechanism from the surface of the bipolar plate and from the surface of the carbon cloth, i.e., this behaviour is defined by the same heat transfer coefficient. Furthermore, since the channel depth is relatively small, the bottom and the top of this rectangular volume are assumed to be at the same temperature. The thermal model of the bipolar plate is shown in Fig. 3.

For the external area of the bipolar plates and the two end blocks exposed to the surroundings, we assume that the convection coefficient is uniform in all directions and that the perimeter of the plate has a uniform temperature, i.e. graphite blocks are treated as ideal black bodies. The total heat loss from a hot body to its surroundings often includes appreciable losses by conduction, convection and radiation [32]. All these phenomena are taken into consideration in the present model, and hence the model can be used to estimate the amount of thermal insulation for the stack.

During cell operation a fraction of the inlet stream is consumed as reactants. Since both fuel and oxidant are in excess, the majority of the exiting streams will, in most situations, remove heat from the cell and leave at elevated temperatures. In addition, CO_2 and water, which are the by-products of the half-cell reactions, also flow out of the gas diffusion layer and thus, remove heat. The above is clearly only valid under the assumption that the outlet temperature of the anode is higher that the inlet, and that the gas diffusion layer is at a higher temperature than the mean temperature of the anode stream. This is not necessary always true. Depending on the stack operating conditions and the number of the cells in the stack heat can also be transferred from the inlet stream to the cell itself.

At this point it is appropriate to consider the heat transfer situation in a qualitative way. The change in the sensible heat of the excess feed/oxidant is attributed to the convective heat transfer mechanism from the bipolar plate and the gas diffusion layer. In addition, we assume that energy flows from the anode to the cathode. This is expected since the anode stream requires heat for the endothermic anodic reaction, when in the cathode side the exothermic reaction produces heat which is removed from the oxidant and possibly from the next anode inlet stream. With the low flow rates in use with the system, and since it is expected that the heat transfer coefficient at the gas cathode side is considerably lower than that at the anode liquid side, the cathode stream is not able to remove all the heat leaving the cathode gas diffusion layer. Thus, we expect heat to be transferred to the next cell through the bipolar plate.

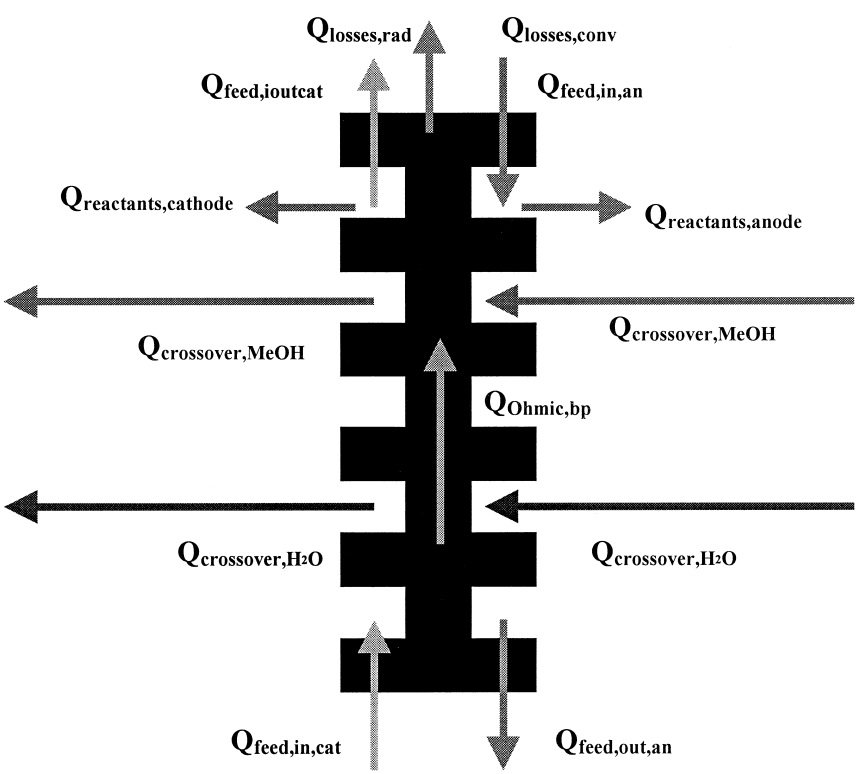

Fig. 3. The heat flows in and out from the bipolar plate.

We can consider the bipolar plates as plane walls of thickness l_{bp}, with uniformly distributed heat sources, and that, under the simplifying assumption, the other dimensions are sufficiently large, the heat flow may be considered as one-dimensional. The differential equation, which governs the heat flow from the cathode to the anode side, is:

$$K_{bp}\frac{d^2T}{dx^2} = \left(h_{air}A_{exp}\left(T_{plate,ext} - T_{env}\right) + \sigma T_{plate,exp}^4 - i^2R_{bp}\right) \quad (12)$$

where K_{bp} is the thermal conductivity of the plate, and R_{bp} is the ohmic resistance per unit volume. The governing equation is rewritten as:

$$\frac{d^2T}{dx^2} = \frac{1}{K_{bp}}\left(A_{exp}(h_{air} + h_r)\left(T_{plate,ext} - T_{env}\right) - i^2R_{bp}\right) \quad (13)$$

which can be rewritten:

$$\frac{d^2T}{dx^2} - \frac{hP}{kA}(T - T_{env}) + \frac{\dot{q}}{k} = 0. \quad (14)$$

4.7. End blocks

The end blocks define that part of the stack structure, before the first cell anode side gas diffusion layer and after the last cell cathode side diffusion layer. Essentially these are the two graphite blocks which have channels machined on only one side, the two current collectors, two electrically and thermally insulating polymer sheets, and finally two stainless steel supporting plates.

A schematic representation of the thermal model for this part of the stack is presented in Fig. 4.

The graphite end blocks are made of the same material as the bipolar plates, although they are of different thickness (e.g., 25 mm instead of 8 mm for the bipolar plates). This means that essentially the same model for the bipolar plates is used in this case, with some minor differences. First of all, the convection heat transfer coefficient is slightly smaller than for the anode and cathode side of the bipolar plates, because the surface temperatures are lower than the ones for the bipolar plates. Another difference is that the greater exposed area, (thicker plate), increases the heat losses to the surroundings compared to the bipolar plates.

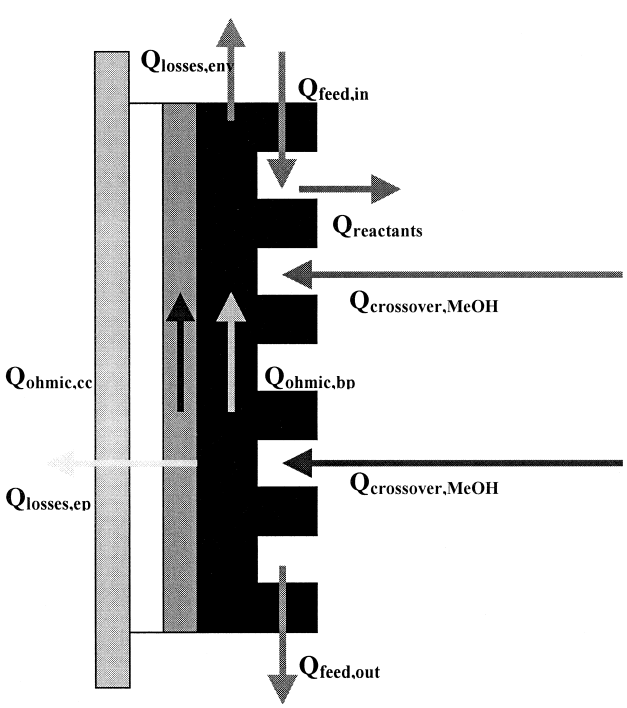

Fig. 4. Schematic representation of the end blocks thermal model.

The current collectors, are relatively thin, and thus assume that there are no heat losses (from convection and radiation heat transfer) to the surroundings. At the same time it produces a relatively small amount of heat due to the low ohmic resistance:

$$\frac{d^2T}{dx^2} = -\frac{i^2 R_{cc}}{K_{cc}} \tag{15}$$

where R_{cc} is the ohmic resistance per unit volume and i is the corresponding current.

The polypropylene insulating sheet and the stainless steel plate can be treated as two plane walls in direct contact, with the preceding current collector. Heat is transferred by conduction. Heat losses to the surroundings from the polypropylene plate, and contact resistance between the two materials are ignored. The governing equation in this case is:

$$\frac{d^2T}{dx^2} = 0. \tag{16}$$

The location of the polymer insulating sheet causes the stainless steel plate to have an almost negligible effect on the thermal model. Although the block is dissipating heat from its side and front face its heat losses to the surrounding environment are small. Nevertheless, heat transfer in the plate is, for completeness, included in the thermal model, i.e.:

$$K_{ssp}\frac{d^2T}{dx^2} - h_{air}A_{exp}(T - T_{env}) = 0. \tag{17}$$

5. Solution strategy

The above component equations of the cell stack model are all combined to model the temperature distribution in the components of the system and the enthalpy flows. The boundary conditions were that between each single component the continuity of heat flow is applied and also an equality of temperature at adjacent surfaces. There are a several input parameters that should be fed into the model in order to fully define the hypothetical stack geometry, the fuel cell electrochemistry, and the materials properties. In addition, the desired number of cells present in the stack and the full set of operating conditions (anode and cathode side inlet temperatures, pressures, and flow rates, the required current density, etc.) also act as model inputs.

The solution procedure adopted is as follows: an initial value is given for the outlet temperature of the anode side of the first cell. The equation of thermal energy conservation is then solved for the region included between the graphite end block and the carbon cloth of the diffusion layer. This gives the value of the diffusion layer inlet temperature. The cathode side temperature is then calculated under the following concept. The convective heat transfer coefficient is based on the temperature gradient of the previous iteration, and hence we are able to calculate from the local energy conservation equation the maximum heat load that the stream can remove. This is also applicable to the anode side outlet temperature of the next cell, since now the gas diffusion layer inlet temperature is known. The model calculates, after each iteration, all the heat flows in or out of each individual cell and from the whole stack body. The model then sums up all these values and forms the stack overall energy balance based on the initial guessed value for the anode side outlet temperature of the first cell. An iterative procedure, based on the net stack energy balance, is used to correct the guessed value and thus give a better approximation. The convergence criterion is set as the difference between the net heat loss/gain from the whole process of two successive iterations to be less than 0.001. Finally new average values for the anode and cathode side outlet temperatures, for the bipolar plate inlet and outlet temperatures and for their exposed area, are calculated in order to improve the accuracy of the calculated heat transfer coefficients, and physical properties. The algorithm is written in Borland C + + and converges quickly in a fast Pentium PC machine after a few decades of iteration.

6. Temperature distribution and heat flow

This section briefly illustrates the temperature distribution and heat flows, which are predicted by the model for a small cell stack. Part II of the paper looks in detail at the influence of operating variables on DMFC cell stack behaviour.

As an example Fig. 5 depicts the temperature profile of a two-cell stack (a two-cell stack was chosen for presentation reasons) operating at the following conditions. For the anode side: 1.0 dm^3 min^{-1} aqueous methanol solution, flow rate per

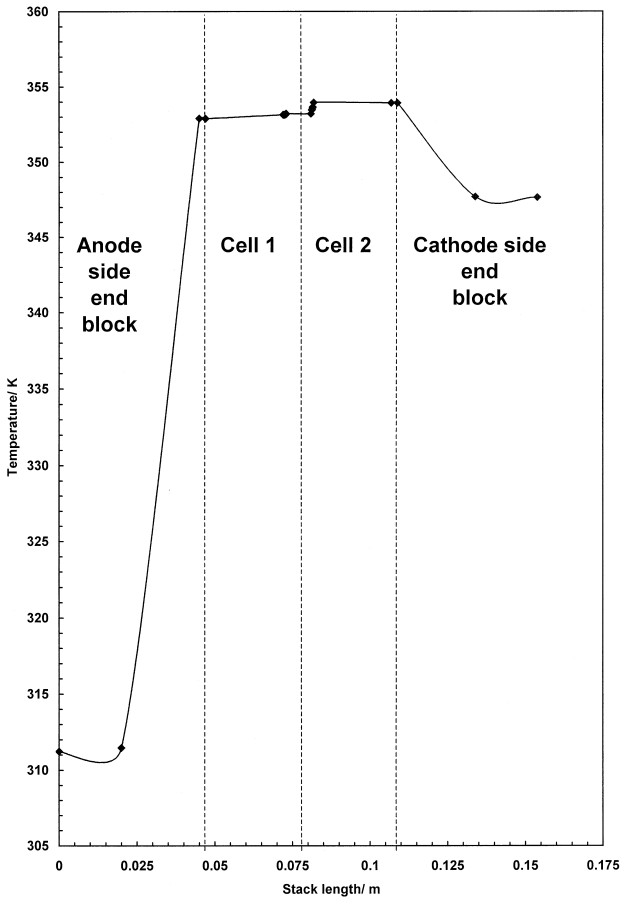

Fig. 5. Predicted temperature profile for a two-cell stack.

cell, 2 M methanol concentration, 80°C solution inlet temperature, and a current density of 100 mA cm^{-2}. Cathode side; 2 bar cathode gauge pressure, 22°C air inlet temperature, and 1.0 dm^3 min^{-1} air flow rate per cell.

The first area labelled anode side end block includes the anode side stainless steel supporting plate, the polymer-insulating sheet, the current collector and the anode side end graphite plate. In this case the stainless steel plate is at a temperature of almost 40°C (first two points in the graph), followed by the polymer sheet which acts sufficiently as an insulator (a gradient of almost 40°C exists). The relatively thin copper current collector sheet follows which is at a temperature of almost 80°C. Adjacent to this dashed line is the end graphite block (it can be seen from the gradient that heat flows from the liquid towards the end blocks). The group of points that follow stands for the MEA, which is too thin in comparison with the rest stack for the points to be clearly distinguished. The next vertical dashed line cuts the bipolar plate in two parts. A very small gradient exists which is evident of some remaining heat transferred from the first cell to the second one. Comparing the second cell MEA with the first, where higher temperature exists we can see the dominant effect that the presence of the anode block has on the heat management and hence the electrical performance of the first cell. It therefore should be expected that the second cell will have a better power output than the first due to the higher temperature. The remaining part is the cathode side end block, which is similar to the anode end block, but is at a higher temperature than the anode block. Overall, heat is flowing from the anode side to the cathode side. Due to insufficient heat removal capacity from the air stream in the last cell cathode side, the heat transfer occurs through the cathode side end block.

Fig. 6 represents the relative heat flow, which occur for a three-cell stack. The operating conditions are the same as above. The average anode side Reynolds number is 186 and for the cathode approximately 6. Thus, the convective heat transfer coefficient is quite low: ≈ 11 W m^{-2} K for the case of the anode and only ≈ 2 W m^{-2} K for the cathode side. We must point out that with the 1:1 ratio of anode to cathode flow rate (1.0 l min^{-1} for both sides) the cathode side air supply is close to the stoichiometric requirement (only 0.046 times excess air). Hence, the low Reynolds number for that stream. The heat transfer coefficient between the exposed area and the environment, and the radiation heat transfer coefficient is less than 1.0 W m^{-2} K^{-1}.

The anode side inlet stream carries a net heat of 75.029 W and leaves the stack with a heat load of 75.007 W, leaving a net heat in the stack of 22.0 W. The cathode side air stream removes 10.57 W (the cathode stream enters with a heat content

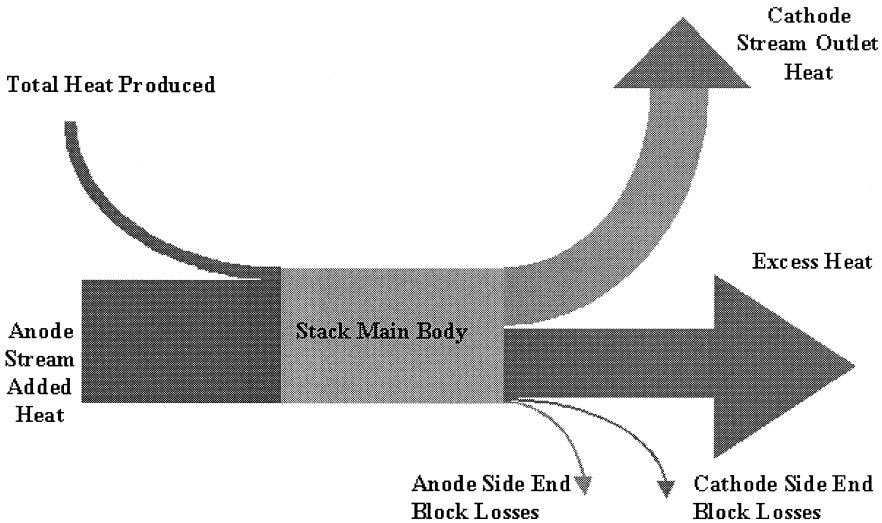

Fig. 6. Energy flows for a three-cell DMFC stack.

of 41.34 W and leaves at 51.92 W). The stack main body (i.e., the stack without the end blocks) produces 1.9 W of heat and 0.42 W accounts for the total heat losses. This heat is from the ohmic resistance of the stack components, plus the overpotential related heat, and the heat of reaction minus the heat losses to the environment, and the heat of water and methanol vaporisation. The anode side end block is responsible for 0.52 W of losses and from the cathode side 0.54 W of heat loss. The total heat produced from all sources in the stack is 2.34 W and the total heat losses account for 1.48 W. An overall heat balance in the stack including the cathode and anode side streams is giving a net heat production from the whole stack of the order of 12.46 W.

Some important points can be made from these calculations. The heat losses from the stack-exposed area tend to be quite small and hence the scope of using an external thermal insulation layer is limited. When the whole system reaches the steady state it can self-sustain each operation with a small heat production. The presence of thermal insulation to all the auxiliary equipment and piping is considered crucial in order to minimise extra heat that is required by an external heater. Finally, for a larger stack it seems that an in-stack-cooling device may be essential for maintaining operating temperature to an acceptable level.

7. Conclusions

A model of the thermal behaviour of the DMFC cell stack is developed, which will enable the variation of the temperature of the various components in the stack as well as the heat flows inside the system to be studied and assessed against operating cell data. The model will also allow an assessment of the thermal requirements for the fuel cell stack operation under practical conditions. The influence of the current and power generated, in relation to the supply and utilisation of the fuel and oxidant, on the operating temperature for maximum power output can be evaluated. The model can be used to predict the steady state performance of the stack for different combinations of operating conditions, the effect of number of cells in the stack, material properties and geometries.

Good knowledge and understanding of the mechanisms governing the stack operation will enable the system's designer to evaluate thermal insulation requirements, to estimate the size of the auxiliary equipment (coolers, and heaters), and to estimate the optimal set of stack operating conditions for a good thermal management.

8. Nomenclature

Symbols

A	Area (m^2)
c_p	Specific heat ($J\ kg^{-1}\ K^{-1}$)

F	Faraday constant (A s mol^{-1})
G	Gibbs free energy (kJ mol^{-1})
H	Reaction enthalpy (kJ mol^{-1})
H	Convective heat transfer coefficient (W m^{-2} K^{-1})
i	Total current (A)
j	Current density (A m^{-2})
k	Thermal conductivity (W m^{-1} K^{-1})
l	Length (m)
m	Mass flow rate (kg s^{-1})
n	Number of electrons transferred through the cell
N	Molar flux (mol s^{-1})
P	Perimeter (m)
Q	Heat (W)
R	Ohmic resistance per unit volume (Ω m^{-3})
S	Entropy (J kg^{-1} K^{-1} mol^{-1})
T	Temperature (K)
x	Coordinate dimension(m)

Subscripts

air	Exposed stack area to air
a	Anode
acl	Anode catalyst layer
agdl	Anode gas diffusion layer
bp	Bipolar plate
c	Cathode
cc	Carbon cloth
ccl	Cathode catalyst layer
cgdl	Cathode gas diffusion layer
env	Surrounding environment conditions
e	Electron/proton
mea	Membrane electrode assembly
mem	Membrane
rev	Reversible

Greek letters

Δ	Change
η	Overpotential (V)
ρ	Resistivity (Ω^{-1} m^{-1})
σ	Stefan Boltzmann constant (W m^{-2} K^{-4})

Acknowledgements

The authors would like to acknowledge the following: (1) the European Commission for supporting Mr. P. Argyropoulos under a TMR Marie Curie research training grant and (2) EPSRC for supporting Dr. W.M. Taama.

Appendix A

The parameters used for the model development in the case of a three-cell DMFC stack are tabulated below.

Number of cells present in stack	3
Feed flow rate (m^3 s^{-1})	5.00e − 05
Concentration of feed solution (M)	2

Feed inlet temperature (K)	353.15
Oxidant flow rate ($m^3\ s^{-1}$)	5.00e − 05
Oxidant pressure (Pa)	200 000
Oxidant inlet temperature (K)	295
Thickness of bipolar plate (m)	0.008
Width of bipolar plate (m)	0.25
Length of bipolar plate (m)	0.25
Channel depth (m)	0.002
Channel width (m)	0.002
Channel separating wall thickness (m)	0.001
Length of MEA (m)	0.16
Width of MEA (m)	0.17
Thickness of anode gas diffusion layer (m)	0.0003
Thickness of cathode gas diffusion layer (m)	0.0003
Thickness of anode catalyst layer (m)	6.50e − 05
Thickness of cathode catalyst layer (m)	6.50e − 05
Thickness of bipolar plate (m)	0.008
Thickness of membrane (m)	0.000175
Thickness of the anode end plate (m)	0.025
Thickness of the cathode end plate (m)	0.025
Thickness of the copper-made current collector (m)	0.002
Thickness of the polymer insulating sheet (m)	0.025
Thickness of supporting steel plates (m)	0.02
Graphite block conductivity ($\Omega^{-1}\ m^{-1}$)	7.50e − 06
Graphite block thermal conductivity ($W\ m^{-1}\ K^{-1}$)	52
Copper-made current collector conductivity ($\Omega^{-1}\ m^{-1}$)	1.67e − 08
Copper-made current collector thermal conductivity ($W\ m^{-1}\ K^{-1}$)	67
Stainless steel end plate thermal conductivity ($W\ m^{-1}\ K^{-1}$)	46
Polymer-made insulating sheet thermal conductivity ($W\ m^{-1}\ K^{-1}$)	0.32
Gas diffusion layer conductivity ($\Omega^{-1}\ m^{-1}$ [33])	72 700
Gas diffusion layer thermal conductivity ($W\ m^{-1}\ K^{-1}$)	0.15
Anode catalyst layer conductivity ($\Omega^{-1}\ m^{-1}$ [33])	72 700
Anode catalyst layer thermal conductivity ($W\ m^{-1}\ K^{-1}$)	0.2
Cathode catalyst layer conductivity ($\Omega^{-1}\ m^{-1}$ [33])	72 700
Cathode catalyst layer thermal conductivity ($W\ m^{-1}\ K^{-1}$)	0.2
Membrane conductivity ($\Omega^{-1}\ m^{-1}$ [33])	20.2
Membrane thermal conductivity ($W\ m^{-1}\ K^{-1}$ [8])	0.21
Required current density ($mA\ cm^{-2}$)	100
$CH_3OH_{(l)}$ enthalpy of formation ($kJ\ mol^{-1}$ [16,21])	− 238.66
$CH_3OH_{(l)}$ Gibbs free energy ($kJ\ mol^{-1}$ [16,21])	− 166.27
$H_2O_{(l)}$ enthalpy of formation ($kJ\ mol^{-1}$ [16,21])	− 298.87
$H_2O_{(l)}$ Gibbs free energy ($kJ\ mol^{-1}$ [16,21])	− 228.6
$H_2O_{(g)}$ enthalpy of formation ($kJ\ mol^{-1}$ [16,21])	− 241.82
$H_2O_{(g)}$ Gibbs free energy ($kJ\ mol^{-1}$ [16,21])	− 237.13
CO_2 enthalpy of formation ($kJ\ mol^{-1}$ [16,21])	− 393.51
CO_2 Gibbs free energy ($kJ\ mol^{-1}$ [16,21])	− 394.0
Anode overpotential (V [18,19])	0.339255
Cathode overpotential (V [18,19])	0.873979
Total stack current (A)	27.2
Environment temperature (K)	290
Total MEA thickness (m)	0.000905
Total stack thickness (m)	0.162715
Bipolar plate cross-sectional area (m^2)	0.0625
Bipolar plate exposed area (m^2)	0.008
End plate exposed area (m^2)	0.025
MEA cross-sectional area (m^2)	0.0272

Hydraulic diameter of the flow channels (m)	0.002
Anode side fluid velocity (m s^{-1})	0.0730994
Cathode side fluid velocity (m s^{-1})	0.0730994
Fuel excess in times	644.89
Oxidant excess in times	3.06608
Anode side channels Reynolds number	186
Cathode side channels Reynolds number	6.14472

References

[1] J.C. Amphlett, R.M. Baumert, R.F. Mann, B.A. Peppley, P.R. Roberge, A. Rodrigues, Parametric modelling of the performance of a 5-kW proton exchange membrane fuel cell stack, Journal of Power Sources 49 (1994) 349–356.
[2] J.C. Amphlett, R.M. Baumert, R.F. Mann, B.A. Peppley, P.R. Roberge, Performance modelling of the Ballard Mark IV solid polymer electrolyte fuel cell: I. Mechanistic model development, Journal of the Electrochemical Society 142 (1) (1995) 1–8.
[3] J.C. Amphlett, R.M. Baumert, R.F. Mann, B.A. Peppley, P.R. Roberge, Performance modelling of the Ballard Mark IV solid polymer electrolyte fuel cell: II. Empirical model development, Journal of the Electrochemical Society 142 (1) (1995) 9–15.
[4] J.C. Amphlett, R.F. Mann, B.A. Peppley, P.R. Roberge, A. Rodrigues, A model predicting transient responses of proton exchange membrane fuel cells, Journal of Power Sources 61 (1996) 183–188.
[5] J.H. Lee, T.R. Lalk, A modelling technique for fuel cell stack systems, ASME Dynamics Systems and Control Division, 1996.
[6] J.H. Lee, T.R. Lalk, A.J. Appleby, Modelling electrochemical performance in large scale proton exchange membrane fuel cell stacks, Journal of Power Sources 70 (1998) 258–268.
[7] J.H. Lee, T.R. Lalk, Modelling fuel cell stack systems, Journal of Power Sources 73 (1998) 229–241.
[8] G. Maggio, V. Recupero, C. Mantegazza, Modelling of temperature distribution in a solid polymer electrolyte fuel cell stack, Journal of Power Sources 62 (1996) 167–174.
[9] T.V. Nguyen, R.E. White, A water and heat management model for proton exchange membrane fuel cells, Journal of the Electrochemical Society 140 (8) (1993) 2178–2186.
[10] P. Argyropoulos, K. Scott, W.M. Taama, Pressure drop modelling for liquid feed direct methanol fuel cells (DMFCs): Part II. Model based parametric analysis, Chemical Engineering Journal (1999) in press.
[11] P. Argyropoulos, K. Scott, W.M. Taama, Pressure drop modelling for liquid feed direct methanol fuel cells (DMFCs): Part I. Model Development, Chemical Engineering Journal (1999) in press.
[12] P. Argyropoulos, K. Scott, W.M. Taama, Modelling reactants and products flow distribution for internally manifolded DMFC stacks, Journal of Fluids Engineering (1998) submitted.
[13] P. Argyropoulos, K. Scott, W.M. Taama, Hydrodynamic modelling of direct methanol fuel cell stacks, Journal of Applied Electrochemistry (1998) submitted.
[14] P. Argyropoulos, K. Scott, W.M. Taama, Modelling pressure distribution and anode/cathode streams chemical composition in direct methanol liquid feed fuel cells (1998) paper submitted to J. Power Sources.
[15] S.D. Srinivansan, B.B. Dave, K.A. Murugesamoorthi, A. Parthasarathy, A.J. Appleby, Overview of fuel cell technology, Fuel Cell Systems, Plenum, New York, 1993, pp. 37–72.
[16] J.M. Smith, Chemical Engineering Kinetics, 3rd International edn., McGraw-Hill, Singapore, 1981.
[17] R.W. Reeve, P.A. Christensen, A. Hamnett, S.A. Haydock, S.C. Roy, Methanol tolerant oxygen reduction catalysts based on transition metal sulphides, Journal of the Electrochemical Society 145 (10) (1998) 3463–3471.
[18] M.K. Ravikumar, Studies on direct methanol fuel cells and nickel–iron batteries, Indian Institute of Science, 1996.
[19] M.K. Ravikumar, A.K. Shukla, Effect of methanol crossover in a liquid feed polymer electrolyte direct methanol fuel cell, Journal of the Electrochemical Society 143 (8) (1996) 2601–2606.
[20] K. Scott, Electrochemical Reaction Engineering, Academic Press, London, 1991.
[21] A.J. Appleby, Characteristics of fuel cells systems, in: L.J.M. Blomen, M.N. Blomen (Eds.), Fuel Cell Systems, Plenum, 1993, pp. 157–173.
[22] B.E. Conway, in: J.O'M. Bockris, B.E. Conway (Eds.), Modern Aspects of Electrochemistry, Chap. 2, No. 3, Butterworth, London, 1964.
[23] R.C. Reid, J.M. Prausnitz, B.E. Poling, The Properties of Gases and Liquids, 4th edn., McGraw-Hill, New York, 1987.
[24] T.A. Zawodzinski, T.E. Springer, J. Davey, J. Valerio, S. Gottesfeld, Water transport properties of fuel cell ionomers, in: R.E.V. White, M.W. Stockel, J.F. Stockel (Eds.), Modelling of Batteries and Fuel Cells, The Electrochemical Society, Pennigton, 1991, pp. 187–196.
[25] T.A. Zawodzinski, S. Gottesfeld, S. Shoichet, T.J. McCarthy, The contact angle between water and the surface of perfluorosulphonic acid membranes, Journal of Applied Electrochemistry 23 (1992) 86–88.
[26] T.A. Zawodzinski, C. Derouin, S. Radzinski, R.J. Sherman, V.T. Smith, T.E. Springer, S. Gottesfeld, Water uptake by and transport through Nafion® 117 membranes, Journal of the Electrochemical Society 140 (4) (1993) 1041–1047.
[27] T.A. Zawodzinski, T.E. Springer, J. Davey, R. Jestel, C. Lopez, J. Valerio, S. Gottesfeld, A comparative study of water uptake by and transport through ionomeric fuel cell membranes, Journal of the Electrochemical Society 140 (7) (1993) 1981–1985.
[28] T.A. Zawodzinski, J. Derouin, J. Valerio, S. Gottesfeld, The water content dependence of electro-osmotic drag in proton-conducting polymer electrolytes, Electrochimica Acta 40 (3) (1995) 297–302.
[29] K. Scott, W.M. Taama, J. Cruickshank, Performance and modelling of a direct methanol solid polymer electrolyte fuel cell, 4th European Symposium on Electrochemical Engineering, Contemporary Trends in Electrochemical Engineering, Prague, 28–30 August 1996.
[30] J. Cruickshank, K. Scott, The degree and effect of methanol crossover in the direct methanol fuel cell, Journal of Power Sources 70 (1998) 40–47.

[31] C.E. Borroni-Bird, Fuel cell commercialisation issues for light duty vehicle applications, Journal of Power Sources 61 (1996) 33–48.
[32] W.L. McCabe, J.C. Smith, P. Harriott, Unit operations of Chemical Engineering, 5th International edn., McGraw-Hill Chemical Engineering Series, McGraw-Hill, Singapore, 1995.
[33] P.S. Kauranen, DMFCF—A Simulation Program For Direct Oxidation Fuel Cells—Document And User's Guide, Helsinki University of Technology, Espoo, Finland, 1996.